

# PCCP

Accepted Manuscript



This is an *Accepted Manuscript*, which has been through the Royal Society of Chemistry peer review process and has been accepted for publication.

*Accepted Manuscripts* are published online shortly after acceptance, before technical editing, formatting and proof reading. Using this free service, authors can make their results available to the community, in citable form, before we publish the edited article. We will replace this *Accepted Manuscript* with the edited and formatted *Advance Article* as soon as it is available.

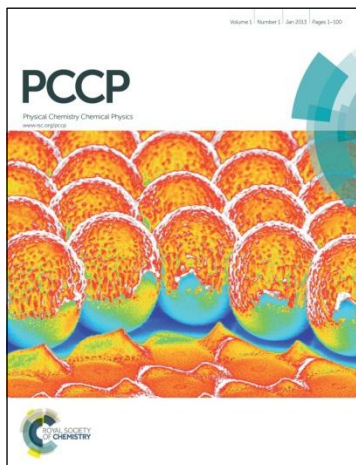
You can find more information about *Accepted Manuscripts* in the [Information for Authors](#).

Please note that technical editing may introduce minor changes to the text and/or graphics, which may alter content. The journal's standard [Terms & Conditions](#) and the [Ethical guidelines](#) still apply. In no event shall the Royal Society of Chemistry be held responsible for any errors or omissions in this *Accepted Manuscript* or any consequences arising from the use of any information it contains.

# PCCP Guidelines for Referees

*Physical Chemistry Chemical Physics* (PCCP) is a high quality journal with a large international readership from many communities

Only very important, insightful and high-quality work should be recommended for publication in PCCP.



**To be accepted in PCCP** - a manuscript must report:

- Very high quality, reproducible new work
- **Important new physical insights** of significant general interest
- A novel, stand-alone contribution

**Routine or incremental work** should not be recommended for publication. Purely synthetic work is not suitable for PCCP

If you rate the article as 'routine' yet recommend acceptance, please give specific reasons in your report.

**Less than 50%** of articles sent for peer review are recommended for publication in PCCP. The current PCCP Impact Factor is **4.20**.

PCCP is proud to be a leading journal. We thank you very much for your help in evaluating this manuscript. Your advice as a referee is greatly appreciated.

With our best wishes,

Anna Simpson ([pccp@rsc.org](mailto:pccp@rsc.org))  
Managing Editor, PCCP

Prof Daniella Goldfarb  
Chair, PCCP Editorial Board

---

**General Guidance (For further details, see the RSC's [Refereeing Procedure and Policy](#))**

Referees have the responsibility to treat the manuscript as confidential. Please be aware of our [Ethical Guidelines](#) which contain full information on the responsibilities of referees and authors.

*When preparing your report, please:*

- Comment on the originality, importance, impact and scientific reliability of the work;
- State clearly whether you would like to see the paper accepted or rejected and give detailed comments (with references) that will both help the Editor to make a decision on the paper and the authors to improve it;

*Please inform the Editor if:*

- There is a conflict of interest;
- There is a significant part of the work which you cannot referee with confidence;
- If the work, or a significant part of the work, has previously been published, including online publication, or if the work represents part of an unduly fragmented investigation.

*When submitting your report, please:*

- Provide your report rapidly and within the specified deadline, or inform the Editor immediately if you cannot do so. We welcome suggestions of alternative referees.

## Response to Decision Letter

Dear Editor:

We would like to thank both the reviewers for reading carefully the manuscript and sharing comments to improve it. Listed below are the modifications/explanations to the reviewers' concerns.

### Reviewer #1:

1) The paper is about analysis of electronic structures at the interface between Au and  $\text{CH}_3\text{NH}_3\text{PbI}_3$  by measurements of UPS and XPS. It contains interesting information for the publication. However, the contents are a bit difficult for the wide range of the readers. Please explain how to obtain the data of Fig. 5 exactly. In order to show the way to get the numeric data for Fig. 5, the authors should describe each value in Fig. 2 and 3 and explain the way to analyze the data.

Ans: We agree with the reviewer that this manuscript is a bit difficult for the wide range of the readers.

We added in Pg. 2, Right column, Line 10 from the bottom the following sentences in order to show the way to get the work function in Fig.2:

“The cut-off energy is determined by the inflection point of the sharp change region of the cut-off spectrum.<sup>23-25</sup> Then the vacuum level (VL) is obtained from the difference between the photon energy (21.22 eV) and the cut-off energy. .”

We added some marks in Fig. 2(a) and Fig. 2(c) to make the numeric data more visible.

We added some explanations for Fig. 3 in Pg. 3, Right column, Line 16 from the bottom:

“All the spectra were normalized to the same height. The BE of the peak center was

obtained by Gaussian fitting. The dash lines mark the core levels C 1s, I 3d and Pb 4f of the pristine  $\text{CH}_3\text{NH}_3\text{PbI}_3$  film.”

We added some descriptions in order to show the way to get the data of Fig. 5 in Pg. 4, Right column, Line 2, 4, 8, 11, 13. In addition, we re-plotted the Fig. 5 to make it clearer for readers.

2) Moreover, the explanations for Fig. 5 and 6 are also not clear. I am sorry, but I couldn't understand the exact meaning of the figures. Please explain using a plain sentences for the scientists who have not worked about UPS and XPS. Afterward, this manuscript will be thought about the publication. .

Ans: We have rewritten the manuscript using plain sentences to the best of our ability in order to make it easy for readers to understand.

We added some explanations for Fig. 6 in Pg. 5, Left column, Line 4, 20 and 24 :

“The photoelectron intensity is obtained by Gaussian fitting of XPS spectra after removing the secondary electron background.”(Line 4)

“The slope curve is obtained by linearly fitting the experimental data of  $\Theta < 8 \text{ \AA}$ . However,”(Line 20)

“the photoelectrons ejected from the  $\text{CH}_3\text{NH}_3\text{PbI}_3$  film are significantly suppressed by the Au coverage and a sharper decrease of photoelectron intensity”(Line 24)

**Reviewer #2:**

This is both a timely and important contribution. The authors have revealed the electronic structure at the interface between gold and the perovskite through UPS and IPES. The authors have established themselves good reputation in the field. It should be published as it is.

Ans: We thank the reviewer for the suggestion.

## Electronic structures at the interface between Au and $\text{CH}_3\text{NH}_3\text{PbI}_3$

Cite this: DOI: 10.1039/x0xx00000x

Xiaoliang Liu,<sup>a</sup> Chenggong Wang,<sup>b</sup> Lu Lyu,<sup>a</sup> Congcong Wang,<sup>b</sup> Zhengguo Xiao,<sup>c</sup> Cheng Bi,<sup>c</sup> Jinsong Huang<sup>c</sup> and Yongli Gao<sup>\*b</sup>,

The electronic properties of interfaces formed between Au and organometal triiodide perovskite ( $\text{CH}_3\text{NH}_3\text{PbI}_3$ ) are investigated using ultraviolet photoemission spectroscopy (UPS), inverse photoemission spectroscopy (IPES) and X-ray photoemission spectroscopy (XPS). It is found that the  $\text{CH}_3\text{NH}_3\text{PbI}_3$  film coated onto the substrate of poly(3,4-ethylenedioxythiophene) poly(styrenesulfonate) (PEDOT:PSS)/indium tin oxide (ITO) by two-step method presents n-type semiconductor behavior, with a band gap of 1.7 eV and a valence band (VB) edge of 1.0 eV below the Fermi energy ( $E_F$ ). An interface dipole of 0.1 eV is observed at  $\text{CH}_3\text{NH}_3\text{PbI}_3/\text{Au}$  interface. The energy levels of  $\text{CH}_3\text{NH}_3\text{PbI}_3$  shift upward by ca. 0.4 eV with Au coverage of 64 Å upon it, resulting in band bending, hence a built-in field in  $\text{CH}_3\text{NH}_3\text{PbI}_3$  that encourages hole transport to the interface. Hole accumulation occurs at the vicinity of the interface, facilitating the hole transfer from  $\text{CH}_3\text{NH}_3\text{PbI}_3$  to Au. Furthermore, the shift of VB maximum of  $\text{CH}_3\text{NH}_3\text{PbI}_3$  toward the  $E_F$  indicates a decrease of energy loss as extracting holes from  $\text{CH}_3\text{NH}_3\text{PbI}_3$  to Au coverage.

Received 00th August 2014,  
Accepted

DOI: 10.1039/x0xx00000x

www.rsc.org/

### 1. Introduction

Recently, there has been an unexpected breakthrough and rapid evolution of highly efficient solid-state hybrid solar cells based on organometal trihalide perovskite materials.<sup>1-8</sup> The breakthrough has the potential to produce solar cells with very high efficiencies while retaining very low cost. Kojima *et al.*<sup>9</sup> first reported in 2009 on a 3.5% efficient sensitized solar cell with  $\text{TiO}_2$ ,  $\text{CH}_3\text{NH}_3\text{PbI}_3$ , and iodide/triiodide redox couple. Im *et al.*<sup>10</sup> improved on the sensitized solar cell by optimizing the  $\text{TiO}_2$  surface and perovskite processing, reporting a 6.5%  $\text{CH}_3\text{NH}_3\text{PbI}_3$  liquid electrolyte solar cell. Kim *et al.*<sup>11</sup> and Lee *et al.*<sup>12</sup> developed solid-state perovskite solar cells employing 2,2',7,7'-tetrakis-(N,N-di-p-methoxyphenyl-amine) 9,9'-spirobifluorene (spiro-OMeTAD) as the hole transporter, and presented efficiencies of between 8% and 10% with  $\text{CH}_3\text{NH}_3\text{PbI}_3$  and  $\text{CH}_3\text{NH}_3\text{PbI}_{3-x}\text{Cl}_x$  mixed halide

perovskite, respectively. By depositing  $\text{PbI}_2$  on nanoporous  $\text{TiO}_2$  and subsequently submerging it into a  $\text{CH}_3\text{NH}_3\text{I}$  solution, Grätzel and his co-workers<sup>13</sup> brought the efficiency to 15%. Using vapor deposition, Snaith's group demonstrated that a planar heterojunction perovskite solar cell, without the mesoporous electrode in typical sensitized solar cells, could have very high efficiency of 15%.<sup>14,15</sup> It is expected that the efficiency of 20% or higher can be reached by optimizing the device structures. In addition, it was also showed one of the most striking aspects of the perovskites that the cells could generate a very high open-circuit voltage ( $V_{oc}$ ), and that the materials exhibited sufficiently good ambipolar charge transport for electrons and holes.<sup>11,16</sup> Given the high efficiency and inexpensive materials and processing, it is forecasted that a new wave of research and development on perovskite solar cells will bring many transformative steps over the coming years and a tangible possibility in making solar energy as the lowest-

cost energy source.

In spite of many achievements in the application of organometal halide perovskite-based organic planar heterojunction solar cells, the basic energetics of these systems still remains unsolved, such as the positions of the electronic band edges and their alignment with the energy levels of adjacent layers. To understand the mechanism and to optimize the device structure of organometal trihalide perovskite-based organic solar cells, it is imperative to learn the precise role of each interface in the device architecture.

In solar cells based on organometal halide perovskite, Au is most widely used as an electrode. It is believed that a typical planar structure of Au/CH<sub>3</sub>NH<sub>3</sub>PbI<sub>3</sub> and an electron transport layer such as C<sub>60</sub>, can be used to build an effective solar cell. To understand the electronic structure and carrier transfer mechanism at the CH<sub>3</sub>NH<sub>3</sub>PbI<sub>3</sub>/Au interface, we report our study using ultraviolet photoemission spectroscopy (UPS), inverse photoemission spectroscopy (IPES) and X-ray photoemission spectroscopy (XPS) on this interface. We measured directly the evolution of energy levels as Au was deposited successively layer by layer on a CH<sub>3</sub>NH<sub>3</sub>PbI<sub>3</sub> film. Au electrode lifted efficiently the energy levels of CH<sub>3</sub>NH<sub>3</sub>PbI<sub>3</sub> and a small energy offset of 0.6 eV was observed between the valence band (VB) edge of CH<sub>3</sub>NH<sub>3</sub>PbI<sub>3</sub> and the Fermi energy (E<sub>F</sub>) of the system, indicating a weak energy loss as holes transfer from CH<sub>3</sub>NH<sub>3</sub>PbI<sub>3</sub> to Au. Au clusters formed on the top of the CH<sub>3</sub>NH<sub>3</sub>PbI<sub>3</sub> film were observed at lower Au coverages, leading to an initial charging of 0.3 eV. These investigations provide some insight to the understanding of Au/CH<sub>3</sub>NH<sub>3</sub>PbI<sub>3</sub>-based organic solar cells.

## 2. Results and discussion

Shown in Fig. 1 is the XPS full scan spectrum of the CH<sub>3</sub>NH<sub>3</sub>PbI<sub>3</sub> film on top of an ITO/PEDOT:PSS substrate. As expected, the sample displays carbon, nitrogen, iodine and lead, and the surface composition C:N:Pb:I = 0.9:0.8:1:2.4 can be confirmed by the core level intensity, indicating a bit of deviation from the stoichiometry of CH<sub>3</sub>NH<sub>3</sub>PbI<sub>3</sub>. We obtained the areas of the XPS spectra of these elements by fitting Gaussian peaks after removing the secondary electron background, followed by normalization with corresponding atomic sensitivity factors. The relatively low proportions of nitrogen, carbon and iodide can be perhaps attributed to the deficiency of CH<sub>3</sub>NH<sub>3</sub>I. The CH<sub>3</sub>NH<sub>3</sub>PbI<sub>3</sub> is not thermally stable at temperatures above 150 °C due to its low dissociation energy.<sup>20-22</sup> Thermal annealing is a necessary step in the fabrication process of perovskite films in order to have enough interdiffusion between CH<sub>3</sub>NH<sub>3</sub>I and PbI<sub>2</sub>. However, thermal annealing may also dissociate partly CH<sub>3</sub>NH<sub>3</sub>PbI<sub>3</sub> into PbI<sub>2</sub> and CH<sub>3</sub>NH<sub>3</sub>I, and the CH<sub>3</sub>NH<sub>3</sub>I may subsequently evaporate, resulting in reduced N content.

In Fig. 2, the evolution of the UPS spectra is presented as a function of the thickness of Au deposited on the CH<sub>3</sub>NH<sub>3</sub>PbI<sub>3</sub> film. For visual clarity, we normalized all the spectra to the same height. Shown in Fig. 2(a) are the UPS data of the cut-off region with the binding energy (BE) from the E<sub>F</sub> of the system. The cut-off energy is determined by the inflection point of the sharp change region of the cut-off spectrum.<sup>23-25</sup> Then the vacuum level (VL) is obtained from the difference between the photon energy (21.22 eV) and the cut-off energy. The VL of CH<sub>3</sub>NH<sub>3</sub>PbI<sub>3</sub> film is measured to be 4.7 eV above the E<sub>F</sub>, *i.e.*, work function (WF), and it decreases to 4.4 eV upon the deposition of 0.5 Å Au. With the subsequent deposition of Au, the VL increases rapidly at first, and then more gradually. It finally saturates at 5.2 eV with Au coverage of

64 Å. Fig. 2(b) presents the UPS data of the highest lying VB regions, in which the VB maximum (VBM) of  $\text{CH}_3\text{NH}_3\text{PbI}_3$  film displays ca. 1.0 eV. The VB edges are obtained using linear extrapolation as illustrated in our previous works.<sup>26,27</sup> As more Au is deposited, a finite density of valence states is observed within the gap of  $\text{CH}_3\text{NH}_3\text{PbI}_3$ . The density of valence states is faint at first, and then it extends up to  $E_F$  as the Au coverage reaches ca. 8 Å and a true metallic Fermi edge develops completely with the Au deposition of up to  $\Theta = 64$  Å. This effect is just similar to that confirmed by Dürr *et al.*<sup>28</sup> as Au was deposited on diindenoperylene (DIP).

Notably, a sharp shift of ca. 0.3 eV toward high BE is observed from the UPS spectra of the cut-off region and the VB edge region at 0.5 Å Au deposition upon  $\text{CH}_3\text{NH}_3\text{PbI}_3$  film, which can be ascribed to sample charging during UPS at lower Au coverage. As reported by Koch *et al.*<sup>29</sup> and Oji *et al.*,<sup>30</sup> Au clusters formed on some organic films as Au was deposited upon them with lower Au overlayer. Here, small Au clusters formed on the top of the  $\text{CH}_3\text{NH}_3\text{PbI}_3$  film make it difficult to transfer electrons from  $\text{CH}_3\text{NH}_3\text{PbI}_3$  to the Au clusters to establish charge neutrality, resulting the Au clusters positive charging of ca. 0.3 eV, hence the same amount of energy level shift toward higher BE. However, upon the subsequent Au deposition, the UPS spectra shift back to lower BE, indicating that thicker Au films eliminate the charging. This process can be interpreted by percolation theory. Most clusters on the top of  $\text{CH}_3\text{NH}_3\text{PbI}_3$  film are too small to be metallic at first, and then an increasing number of the clusters become large enough to percolate, thus to exhibit metallic character. Shown in Fig. 2(c) is the local enlarged view of the VB edge region near  $E_F$ . We observe here that the Fermi edge actually is visible even for 2 Å of Au. At this phase the Fermi edge locates 0.2 eV below the  $E_F$  of the system due to the charging. During the process of the subsequent Au deposition, it shifts back toward the  $E_F$

because of the elimination of the charging induced by the Au clusters percolation (see the dotted lines in Fig. 2(c)). Upon the deposition of ca. 8 Å Au, the shift of the Fermi edge almost saturates and a continuous metal surface coverage and conductivity are achieved.

To obtain the detailed information of the unoccupied states of  $\text{CH}_3\text{NH}_3\text{PbI}_3$ , we further collected the IPES data of the pristine  $\text{CH}_3\text{NH}_3\text{PbI}_3$  film. The IPES spectrum is presented in Fig. 2(d). The conduction band minimum (CBM) is measured to be 0.7 eV above the Fermi level ( $E_F$ ), while the VBM 1.0 eV below the  $E_F$ , corresponding to a gap of 1.7 eV, which is consistent with previous reports.<sup>31</sup> Interestingly, the  $\text{CH}_3\text{NH}_3\text{PbI}_3$  film measured here presents an n-type semiconductor behavior. It is possible that the conductivity type, *i.e.*, n-type or p-type, can be tuned by the film formation composition and thermal annealing process.

The positive charging induced by Au clusters at lower Au coverage is also confirmed by the XPS spectra. Shown in Fig. 3 are the evolutions of C 1s, I 3d, Pb 4f and Au 4f XPS peaks as a function of increasing Au coverage. All the spectra were normalized to the same height. The BE of the peak center was obtained by Gaussian fitting. The dash lines mark the core levels C 1s, I 3d and Pb 4f of the pristine  $\text{CH}_3\text{NH}_3\text{PbI}_3$  film. In Fig. 3(a), 3(b) and 3(c), the core levels of C 1s, I 3d and Pb 4f shift simultaneously  $0.3 \pm 0.1$  eV toward higher BE resulting from the initial charging at  $\Theta = 0.5$  Å. Then, following the same manner of the VL and the VBM of  $\text{CH}_3\text{NH}_3\text{PbI}_3$  presented by UPS spectra, they shift toward lower BE with more Au deposition as the charging is being eliminated. It is observed that a Au coverage of about 8 Å can eliminate the charging and shift the core levels of C 1s, I 3d and Pb 4f back to the original position of the pristine  $\text{CH}_3\text{NH}_3\text{PbI}_3$  film. In addition, as shown in Fig. 3(d), the evolution of Au 4f peak provides further evidence for the positive

charging. We obtained the highest BE of Au 4f at the initial  $\Theta = 0.5 \text{ \AA}$  of Au coverage due to the positive charging, then this core level shifts downward gradually as the charging is gradually eliminated by further Au depositions. Moreover, we also observed the broadening of the XPS spectra at  $\Theta = 0.5\text{--}2 \text{ \AA}$  of Au deposition, which is another evidence supporting the existence of Au clusters.<sup>28</sup> Notably, the core levels of C 1s, I 3d and Pb 4f shift back to lower BE by ca. 0.4 eV with Au coverage of  $64 \text{ \AA}$  relative to the pristine  $\text{CH}_3\text{NH}_3\text{PbI}_3$  film.

In Fig. 4, we present directly the relative shifts of the VL and core levels at the  $\text{CH}_3\text{NH}_3\text{PbI}_3/\text{Au}$  interface as a function of Au coverage. The core levels of C 1s, I 3d and Pb 4f shift almost the same as the VL, indicating no significant surface chemical modification during this deposition process. As discussed in the previous section, the energy levels shift toward higher BE upon small Au depositions, and shift back to the original position with Au coverage of ca.  $8 \text{ \AA}$  due to the elimination of charging. They then shift sequentially toward lower BE with enough thickness of Au deposition.

Generally, to obtain the true information of the energy level positions, the charging effect must be removed. Koch *et al.*<sup>32</sup> introduced a technique to eliminate the charging by irradiating the sample with light of appropriate wavelength. But in this paper, it is unnecessary to eliminate the charging by using extra technique since the charging is naturally eliminated with the Au deposition of up to  $8 \text{ \AA}$  and the impact of the charging on energy level can be ignored with enough Au coverage. The rigid shifts of core levels saturated at ca. 0.4 eV lower BE with respect to the initial core levels in  $\text{CH}_3\text{NH}_3\text{PbI}_3$  film, indicating the shift upward of energy levels, thus, the band bending in  $\text{CH}_3\text{NH}_3\text{PbI}_3$  film induced by the Au coverage.

The energy level alignment diagram at  $\text{CH}_3\text{NH}_3\text{PbI}_3/\text{Au}$

interfaces is depicted in Fig. 5. The VL and CBM of pristine  $\text{CH}_3\text{NH}_3\text{PbI}_3$  film gotten from Fig. 2(a) and 2(d) are 4.7 and 0.7 eV above the  $E_F$ , respectively, while the VBM gotten from Fig. 2(b) is 1.0 eV below the  $E_F$ . A gradual energy level shift is observed with the subsequent Au depositions. We neglected the intermediate charging processes because it was naturally eliminated without a significant impact on the final energy levels. On the side of  $\text{CH}_3\text{NH}_3\text{PbI}_3$ , at the very interface of  $\text{CH}_3\text{NH}_3\text{PbI}_3/\text{Au}$ , the VL, CBM and VBM of  $\text{CH}_3\text{NH}_3\text{PbI}_3$  are 5.1, 1.1 eV above, and 0.6 eV below the  $E_F$ , respectively, after considering the 0.4 eV upward shift of energy levels with respect to the final deposition of  $64 \text{ \AA}$  Au. On the side of Au, the VL is 5.2 eV according to the UPS data in Fig. 2, which indicating that there is an interface dipole of 0.1 eV at the interface of  $\text{CH}_3\text{NH}_3\text{PbI}_3/\text{Au}$  ascribed to the difference of WF between  $\text{CH}_3\text{NH}_3\text{PbI}_3$  and Au. The VBM of  $\text{CH}_3\text{NH}_3\text{PbI}_3$  is brought to the  $E_F$  of the system, resulting in a band bending as mentioned in previous subsection, and thus a built-in field in the  $\text{CH}_3\text{NH}_3\text{PbI}_3$  film that encourages hole transport to the interface. The hole accumulation at the vicinity of the interface facilitates the hole transfer from  $\text{CH}_3\text{NH}_3\text{PbI}_3$  to Au. Furthermore, the decreasing energy offset between the VBM of  $\text{CH}_3\text{NH}_3\text{PbI}_3$  and the  $E_F$  indicates a decreasing energy loss for hole extraction from  $\text{CH}_3\text{NH}_3\text{PbI}_3$  to the Au. Given the favorable energy level alignment, the  $\text{CH}_3\text{NH}_3\text{PbI}_3/\text{Au}$  interface can be effectively used as holes collector in perovskite-based solar cells.

In order to further ascertain the process of the growth of Au on  $\text{CH}_3\text{NH}_3\text{PbI}_3$  film, we focus on the XPS intensity attenuation by the Au overlayer. For the elements in the  $\text{CH}_3\text{NH}_3\text{PbI}_3$  substrate, the intensity attenuation of photoelectrons after passing through a Au overlayer of thickness  $d$  is given by<sup>33</sup>

$$I_s = I_{s,0} \exp(-d/\lambda_s), \quad (1)$$



where  $I_{s0}$  and  $I_s$  are the original and attenuated photoelectron intensity, respectively,  $\lambda_s$  the mean free path (MFP) of photoexcited electrons in Au.

The photoelectron intensity is obtained based on the peak area and after proper normalization using atomic sensitivity factors. As shown in Fig. 6, for the photoelectrons ejected from the C 1s, I 3d and Pb 4f in the  $\text{CH}_3\text{NH}_3\text{PbI}_3$  film, the intensities attenuate gradually with increasing the thickness of Au coverage up to 8 Å, and decrease sharply with thicker Au coverage, which can be also attributed to the effect of Au clusters. The slight differences in shape among the three curves arise from the slightly different kinetic energies of the electrons ejected from the three core levels. The formation of Au clusters at lower Au coverages, i.e.  $\Theta < 8\text{Å}$ , exposes a larger surface area of the underlying  $\text{CH}_3\text{NH}_3\text{PbI}_3$  film than an evenly distributed Au film, thereby the photoelectron intensity decreases gently at first, which can be confirmed by a small slope for the C 1s as shown with a dash line in the figure. The slope curve is obtained by linearly fitting the experimental data of  $\Theta < 8\text{Å}$ . However, with enough thickness of the Au coverage, i.e.  $\Theta > 8\text{Å}$ , the Au clusters percolates and a continuous metal Au surface coverage is formed on the top of the  $\text{CH}_3\text{NH}_3\text{PbI}_3$  film. Thus, the photoelectrons ejected from the underlying  $\text{CH}_3\text{NH}_3\text{PbI}_3$  film are significantly suppressed by the Au coverage and a sharper decrease of photoelectron intensity is certainly achieved with subsequent deposition of Au, which can also be confirmed by a relative bigger slope for the C 1s as shown with a dash dotted line in the figure.

### 3. Experimental method

#### Preparation of $\text{CH}_3\text{NH}_3\text{PbI}_3$ film

$\text{CH}_3\text{NH}_3\text{PbI}_3$  film was prepared by using a two steps technique as recently reported.<sup>13,17-19</sup> Shortly, poly(3,4-

ethylenedioxythiophene) poly(styrenesulfonate) (PEDOT:PSS) was spun coated onto the ITO substrate at 3000 rpm for 60 s, and then followed by 135 °C annealing for 20min.  $\text{PbI}_2$  precursor solution obtained by dissolving  $\text{PbI}_2$  in anhydrous DMF was spun on to ITO/PEDOT:PSS substrate at 70 °C with 6000 rpm for 45 s, and the as-prepared  $\text{PbI}_2$  film was then dried at 70 °C for 15 min. The  $\text{CH}_3\text{NH}_3\text{I}$  layer was prepared by spin coating the  $\text{CH}_3\text{NH}_3\text{I}$  precursor solution obtained by dissolving  $\text{CH}_3\text{NH}_3\text{I}$  in 2-propanol onto the top of  $\text{PbI}_2$  film at a rate of 6000 rpm for 35 s at room temperature. After the deposition of  $\text{CH}_3\text{NH}_3\text{I}$  layer, the  $\text{PbI}_2/\text{CH}_3\text{NH}_3\text{I}$  stacking film was dried at a hot plate at 75 °C for 15 min, and then annealed at 105 °C for 2 hours.

#### Materials characterization

Au was degassed at proper temperatures before evaporation. 0~64 Å Au films were thermally evaporated layer by layer in the metal evaporation chamber onto ITO/PEDOT:PSS/ $\text{CH}_3\text{NH}_3\text{PbI}_3$  (see inset in Fig. 1). The thickness of evaporated film was monitored with a quartz crystal microbalance. The deposition rate of Au was 0.2 Å/s. The UPS and XPS spectra were recorded at each step, while IPES spectra were just collected for as-grown  $\text{CH}_3\text{NH}_3\text{PbI}_3$  film. The XPS and UPS experiments were performed using a VG ESCA Lab system equipped with a He I (21.2 eV) gas discharge lamp and a Mg  $K_{\alpha}$  X-ray source (1253.6 eV). The IPES spectra were recorded using a custom-made spectrometer, composed of a commercial Kimball Physics ELG-2 electron gun and a band pass photon detector. The photon detector worked in the isochromatic mode centered at a fixed energy of 9.8 eV. The instrumental resolution for UPS measurements was chosen to be 0.20 eV and the XPS resolution is ca. 1.4 eV. The combined resolution (electron + photon) of IPES spectrometer was determined to be ca. 0.6 eV. All measurements were done at room temperature.

**Captions:**

Fig. 1. X-ray photoelectron spectroscopy of the  $\text{CH}_3\text{NH}_3\text{PbI}_3$  film on the top of ITO/PEDOT:PSS substrate. Inset: the schematic diagram of the structure of ITO/PEDOT:PSS/ $\text{CH}_3\text{NH}_3\text{PbI}_3$ /Au.

Fig. 2. Thickness dependent UPS spectra of Au on  $\text{CH}_3\text{NH}_3\text{PbI}_3$  coated on PEDOT:PSS/ITO substrate showing (a) the cut-off region, (b) the VB edge region, (c) the local enlarged view of the VB edge region near  $E_F$ . (d) presents IPES spectra of the density of states close to the bandgap of the  $\text{CH}_3\text{NH}_3\text{PbI}_3$ . Positions of the VB edge and the CB edge are marked with vertical bars, while positions of the cut-off energy and the Fermi edge are marked with dashed and dotted lines, respectively.

Fig. 3. The evolution of (a) C 1s, (b) I 3d and (c) Pb 4f XPS peaks in the  $\text{CH}_3\text{NH}_3\text{PbI}_3$  film, and that of (d) Au 4f XPS peaks in Au coverage, with the increasing Au coverage thickness.

Fig. 4. The relative shifts of vacuum level and core levels at the  $\text{CH}_3\text{NH}_3\text{PbI}_3$ /Au interface deduced from UPS and XPS. The zero of the energy scale refers to the value of zero (or 0.5 Å for Au 4f) Au coverage.

Fig. 5. The energy level diagram of  $\text{CH}_3\text{NH}_3\text{PbI}_3$ /Au interface. The dash dotted lines denote the energy levels of the pristine  $\text{CH}_3\text{NH}_3\text{PbI}_3$  film, while the solid lines on the

side of  $\text{CH}_3\text{NH}_3\text{PbI}_3$  denote the evolution of the energy levels with the deposition of Au.

Fig. 6. The photoelectron intensity as a function of the thickness of Au coverage. The dash line and the dash dotted line mark the slopes for the C 1s before and after the Au deposition of 8 Å, respectively.

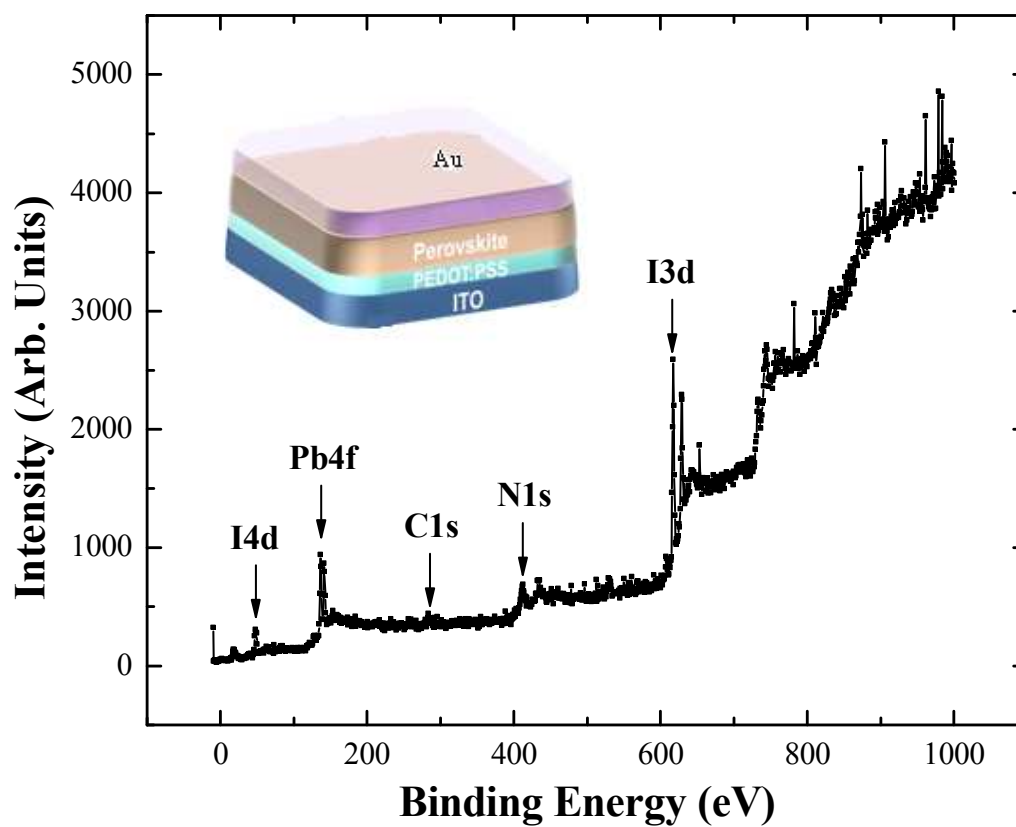


Fig. 1.

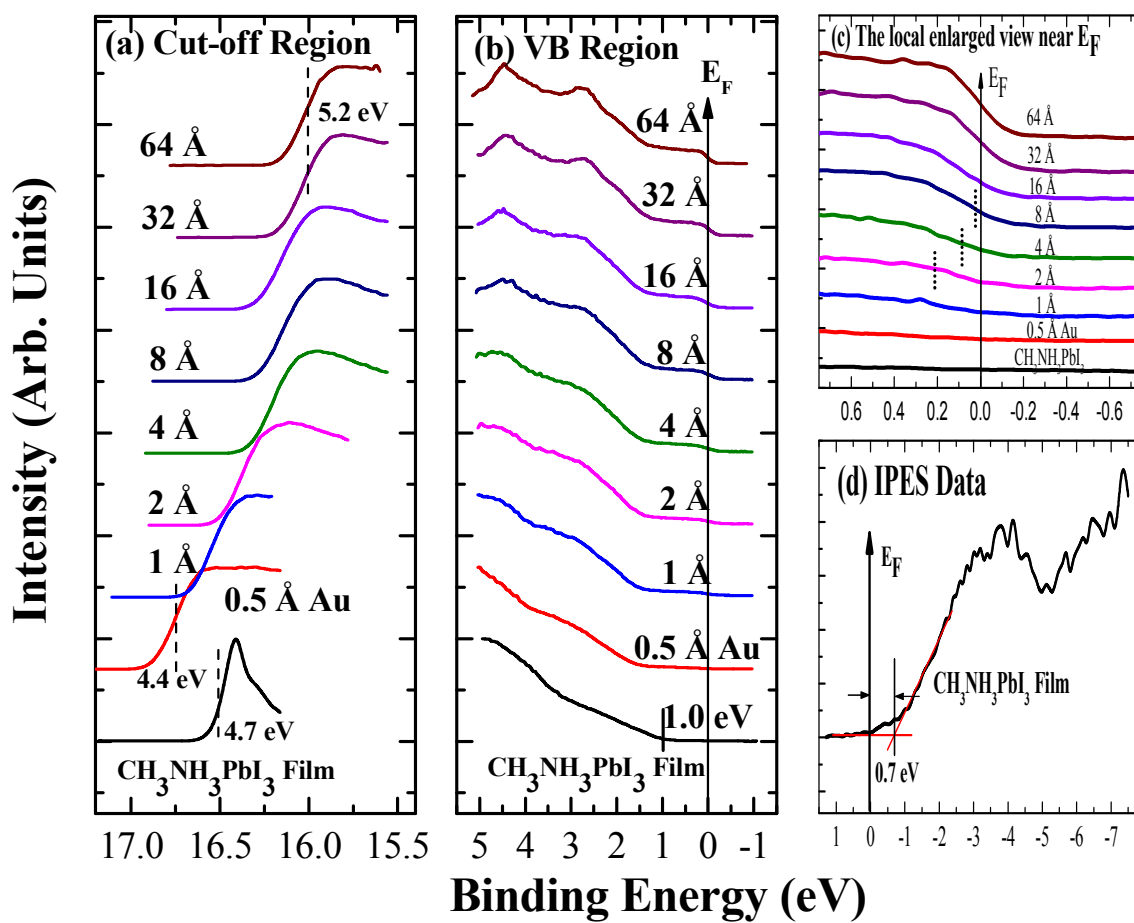


Fig. 2.

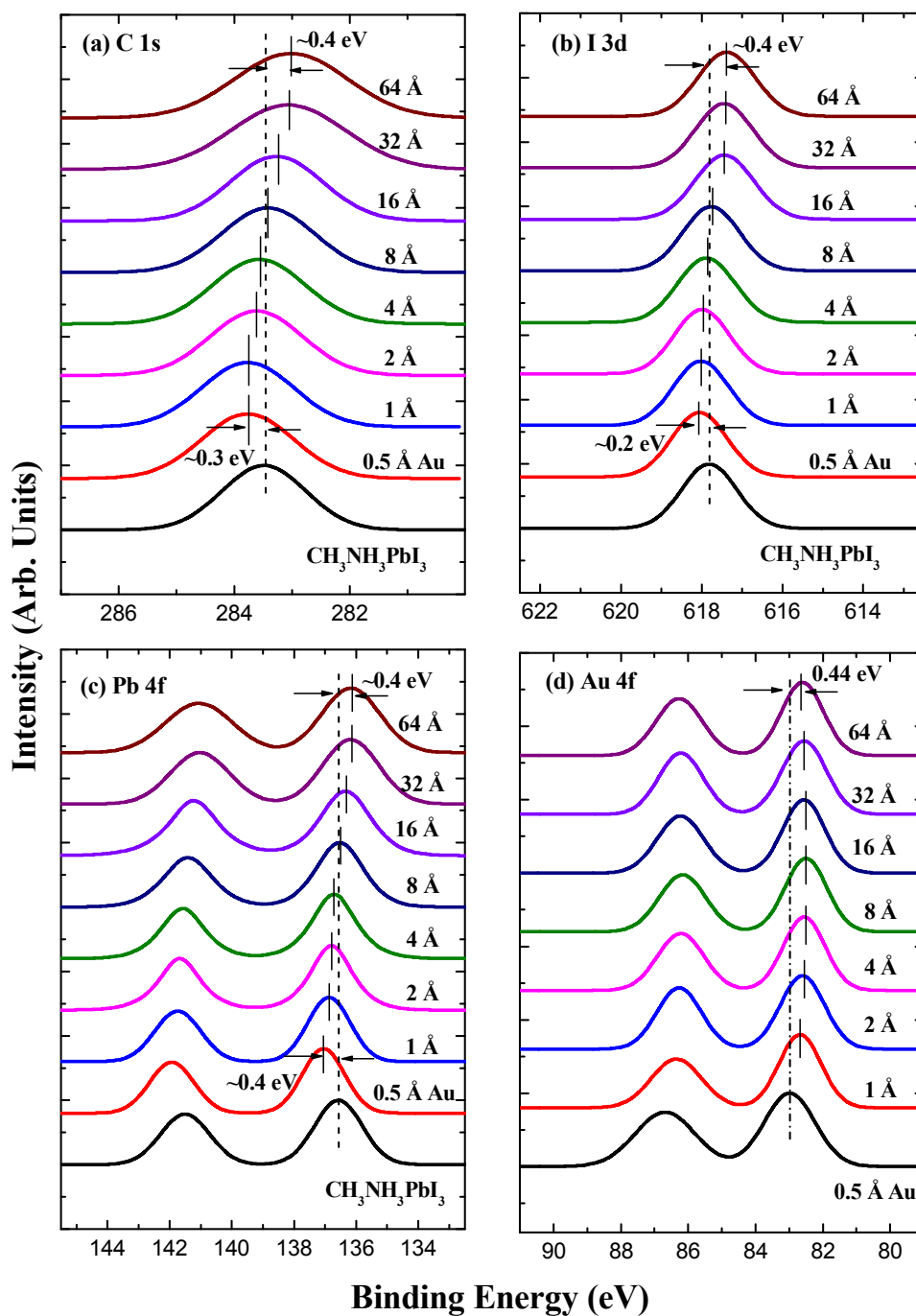


Fig. 3.

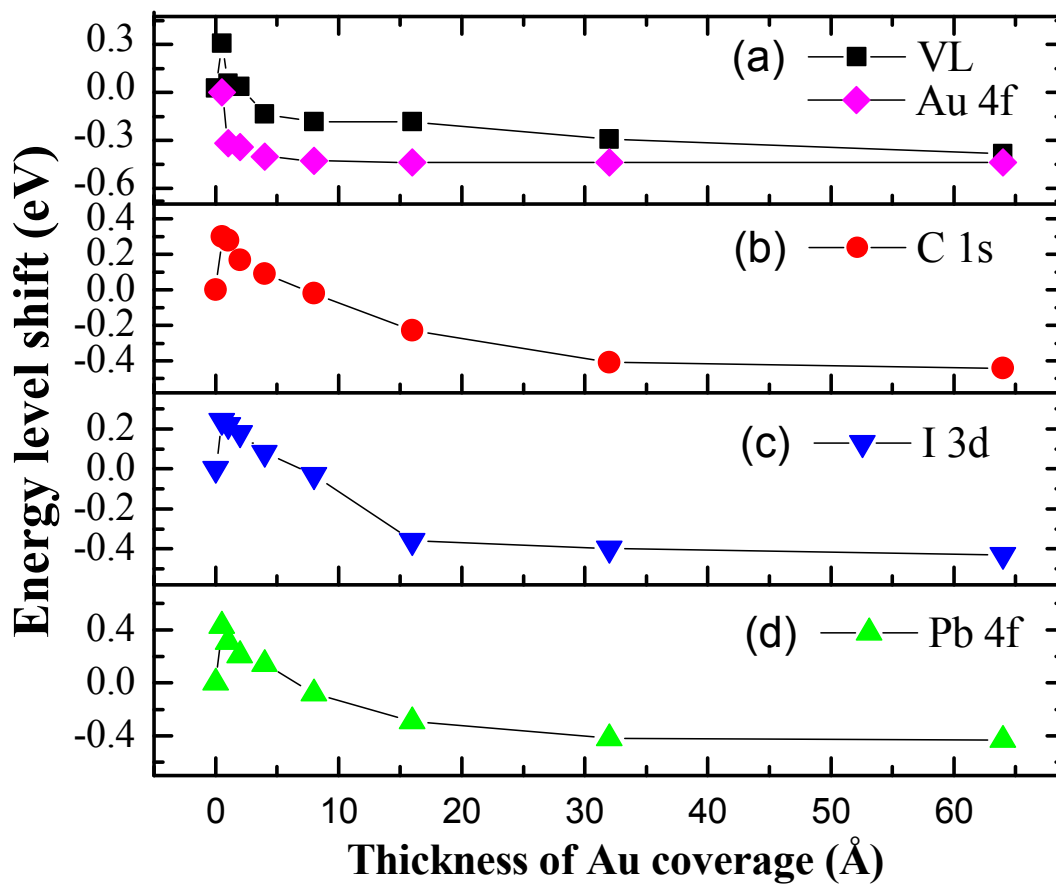


Fig. 4.

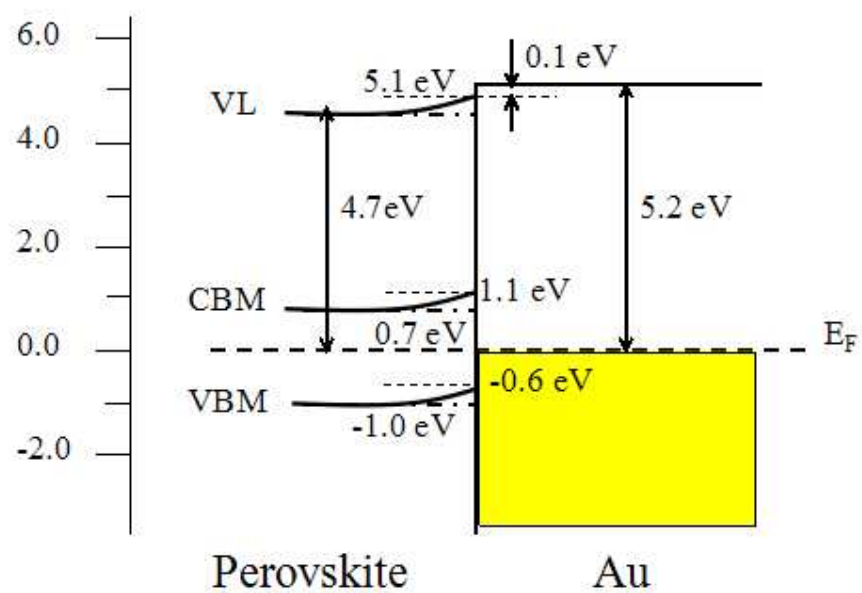


Fig. 5.

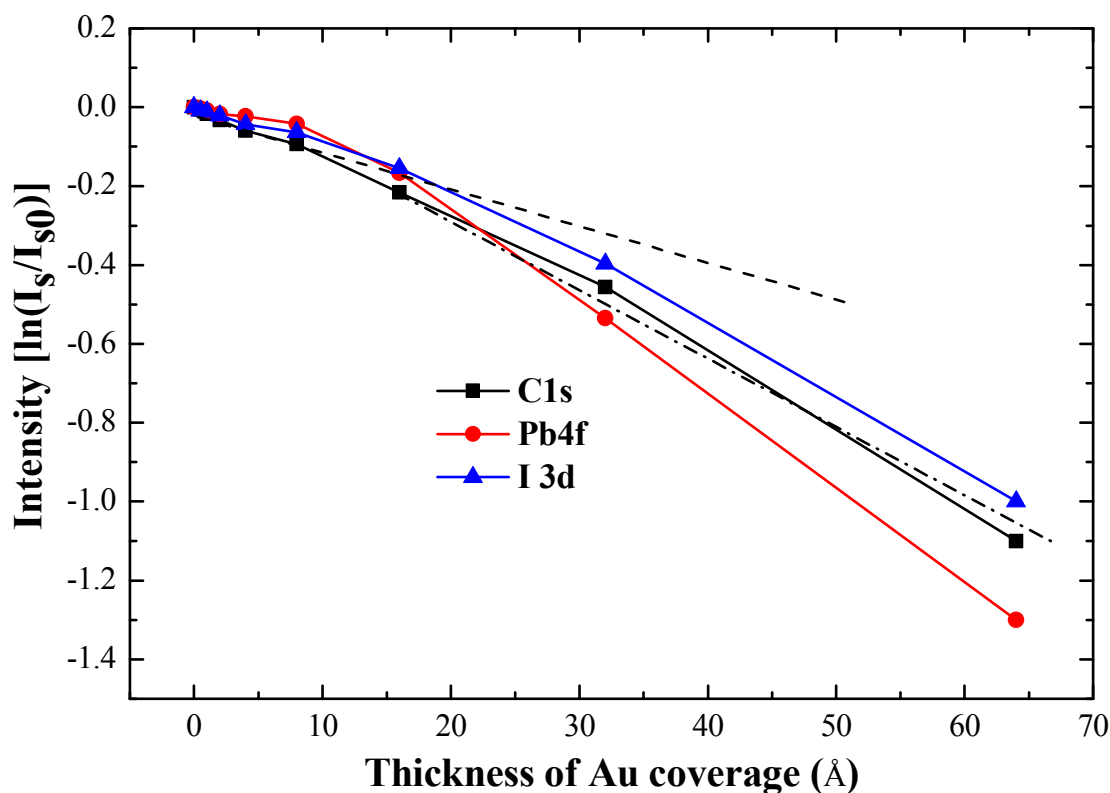


Fig. 6.

#### 4. Conclusions

In conclusion, we have investigated the electronic properties of  $\text{CH}_3\text{NH}_3\text{PbI}_3/\text{Au}$  interface using UPS, XPS and IPES. Au can efficiently lift the energy level of  $\text{CH}_3\text{NH}_3\text{PbI}_3$  film by 0.4 eV, resulting in a band bending and thus a built-in field in  $\text{CH}_3\text{NH}_3\text{PbI}_3$ . The enhanced hole accumulation at the very interface due to the p-type self-doping behavior facilitates the hole transfer from  $\text{CH}_3\text{NH}_3\text{PbI}_3$  to Au. The energy loss decreases significantly as hole extracting from  $\text{CH}_3\text{NH}_3\text{PbI}_3$  to Au electrode due to the decreasing offset between the VBM of  $\text{CH}_3\text{NH}_3\text{PbI}_3$  and the  $E_F$  of the system. Even though for an n-typed  $\text{CH}_3\text{NH}_3\text{PbI}_3$ , it is confirmed that the  $\text{CH}_3\text{NH}_3\text{PbI}_3/\text{Au}$  interface can be effectively used as holes collector in a perovskite-based solar cell, indicating a huge potential of  $\text{CH}_3\text{NH}_3\text{PbI}_3/\text{Au}$ -based organometal trihalide

perovskite planar structured solar cells. Furthermore, an initial charging of 0.3 eV observed with the deposition of lower Au coverage can be attributed to Au clusters formed on the top of the  $\text{CH}_3\text{NH}_3\text{PbI}_3$  film. The charging will be eliminated with thicker Au coverage of ca.  $8\text{\AA}$  following a metallic Fermi edge emergence. These investigations provide some insight to the understanding of  $\text{CH}_3\text{NH}_3\text{PbI}_3/\text{Au}$ -based organic planar heterojunction solar cells.

#### Acknowledgements

This work is supported in part by the National Science Foundation (Grant No. CBET-1437656) and the National Natural Science Foundation of China (Grant No. 51173205, 11334014). One of us (X. L. Liu) acknowledges support by the Natural Science Foundation of Hunan



Province, China (Grant No. 12JJ3003) and the Freedom Explore Program of Central South University, China (Grant No. 2011QNZT122).

## Notes and references

<sup>a</sup>Hunan Key Laboratory for Super-microstructure and Ultrafast Process, College of Physics and Electronics, Central South University, Changsha, 410083, P. R. China

<sup>b</sup>Department of Physics and Astronomy, University of Rochester, Rochester, NY 14627, USA

<sup>c</sup>Department of Mechanical and Materials Engineering and Nebraska Center for Materials and Nanoscience, University of Nebraska-Lincoln, Lincoln, Nebraska 68588-0656, USA

- 1 E. Edri, S. Kirmayer, D. Cahen and G. Hodes, *J. Phys. Chem. Lett.*, 2013, **4**, 897-902.
- 2 P. Docampo, J. M. Ball, M. Darwich, G. E. Eperon and H. J. Snaith, *Nat. Commun.*, 2013, **4**, 2761.
- 3 J.-H. Qiu, Y.-C Qiu, K.-Y. Yan, M. Zhong, C. Mu, H. Yan and S.-H. Yan, *Nanoscale*, 2013, **5**, 3245-3248.
- 4 L. Etgar, P. Gao, Z.-S. Xue, Q. Peng, A. K. Chandiran, B. Liu, M. K. Nazeeruddin and M. Grätzel, *J. Am. Chem. Soc.*, 2012, **134**, 17396–17399.
- 5 D. B Mitzi, S. Wang, C. A. Feild, C. A. Chess and A. M. Guloy, *Science*, 1995, **267**, 1473–1476.
- 6 J.-Y. Jeng, Y.-F. Chiang, M.-H. Lee, S.-R. Peng, T.-F. Guo, P. Chen and T.-C. Wen, *Adv. Mater.*, 2013, **25**, 3727-3732.
- 7 G. C Xing, N. Mathews, S. Y. Sun, S.-S. Lim, Y.-M. Lam, M. Grätzel, S. Mhaisalkar and T. -C. Sum, *Science*, 2013, **342**, 344-347.
- 8 J. A. Mikroyannidis, A. N. Kabanakis, S. S. Sharma and G. D. Sharma, *Adv. Funct. Mater.*, 2011, **21**, 746-755.
- 9 A. Kojima, K. Teshima, Y. Shirai and T. Miyasaka, *J. Am. Chem. Soc.*, 2009, **131**, 6050.
- 10 J. H. Im, C. R. Lee, J. W. Lee, S. W. Park and N. G. Park, *Nanoscale*, 2011, **3**, 4088–4093.
- 11 H. S. Kim, C. R. Lee, J. H. Im, K. B. Lee, T. Moehl, A. Marchioro, S. J. Moon, R. Humphry-Baker, J. H. Yum, J. E. Moser, M. Grätzel and N. G. Park, *Sci. Rep.*, 2012, **2**, 591.
- 12 M. M. Lee, J. Teuscher, T. Miyasaka, T. N. Murakami and H. J. Snaith, *Science*, 2012, **338**, 643–647.
- 13 U. Bach, D. Lupo, P. Comte, J. E. Moser, F. Weissortel, J. Salbeck, H. Spreitzer and M. Grätzel, *Nature*, 1998, **395**, 583–585.
- 14 J. M. Ball, M. M. Lee, A. Hey and H. J. Snaith, *Energy Environ. Sci.*, 2013, **6**, 1739–1743.
- 15 M. Liu, M. B. Johnston and H. J. Snaith, *Nature*, 2013, **501**, 395.
- 16 H. J. Snaith, *J. Phys. Chem. Lett.*, 2013, **4**, 3623-3630.
- 17 J. Burschka, N. Pellet, S. J. Moon, R. Humphry-Baker, P. Gao, M. K. Nazeeruddin and M. Grätzel, *Nature*, 2013, **499**, 316.
- 18 Q. Wang, Y. C. Shao, Q. F. Dong, Z. G. Xiao, Y. B. Yuan and J. S. Huang, *Energy Environ. Sci.*, 2014, **2**, 2359.
- 19 Z. G. Xiao, C. Bi, Y. C. Shao, Q. F. Dong, Q. Wang, Y. B. Yuan, C. G. Wang, Y. L. Gao and J. S. Huang, *Energy Environ. Sci.*, 2014, **7**, 2619-2623.
- 20 C. Bi, Y. Shao, Y. Yuan, Z. Xiao, C. Wang, Y. Gao, and J. Huang, *J. Mater. Chem. A*, 2014, **2**, 18508.

21. A. Dualeh, N. Tétreault, T. Moehl, P. Gao, M. K. Nazeeruddin and M. Grätzel, *Adv. Func. Mater.*, 2014, **24**, 3250-3258. Science and Technology for Photonic and Optoelectronic Applications, Marcel Dekker, New York, 2001.
22. Q. Chen, H. Zhou, Z. Hong, S. Luo, H. Duan, H. Wang, Y. Liu, G. Li and Y. Yang, *J. Am. Chem. Soc.*, 2014, **136**, 622–625
- 23 X. L. Liu, C. G. Wang, I. Irfan, S. J. Yi and Y. Gao, *Org. Electron.*, 2014, **15**, 977.
- 24 X. Liu, S. Yi, C. Wang, C. Wang and Y. Gao, *J. Appl. Phys.*, 2014, **115** (16), 163708.
- 25 Irfan, A. J. Turinske, Y. Z. Bao and Y. Gao, *Appl. Phys. Lett.*, 2012, **101**, 093305.
- 26 Irfan, H. Ding, Y. Gao, C. Small, D. Y. Kim, J. Subbiah and F. So, *Appl. Phys. Lett.*, 2010, **96**, 243307.
- 27 Y. Gao, *Materials Science & Engineering R-Reports*, 2010, **68** (3), 39-87.
- 28 A. C. Dürr, N. Koch, M. Kelsch, A. Rühm, J. Ghijsen, R. L. Johnson, J.-J. Pireaux, J. Schwartz, F. Schreiber, H. Dosch and A. Kahn, *Phys. Rev. B*, 2003, **68**, 115428.
- 29 N. Koch, A.C. Dürr, J. Ghijsen, R.L. Johnson, J.-J. Pireaux, J. Schwartz, F. Schreiber, H. Dosch and A. Kahn, *Thin Solid Films*, 2003, **441**, 145-149.
- 30 H. Oji, E. Ito, M. Furuta, H. Ishii, Y. Ouchi and K. Seki, *Synthetic Metals*, 2001, **121**, 1721-1722.
- 31 P. Schulz, E. Edri, S. Kirmayer, G. Hodes, D. Cahen and A. Kahn, *Energy Environ. Sci.*, 2014, **7**, 1377.
- 32 N. Koch, D. Pop, R.L. Weber, N. Böwering, B. Winter, M. Wick, G. Leising, I. V. Hertel and W. Braun, *Thin Solid Films*, 2001, **391**, 81.
- 33 W.R. Salaneck, K. Seki, A. Kahn, and J.J. Pireaux (Eds.), *Conjugated Polymer and Molecular Interfaces:*

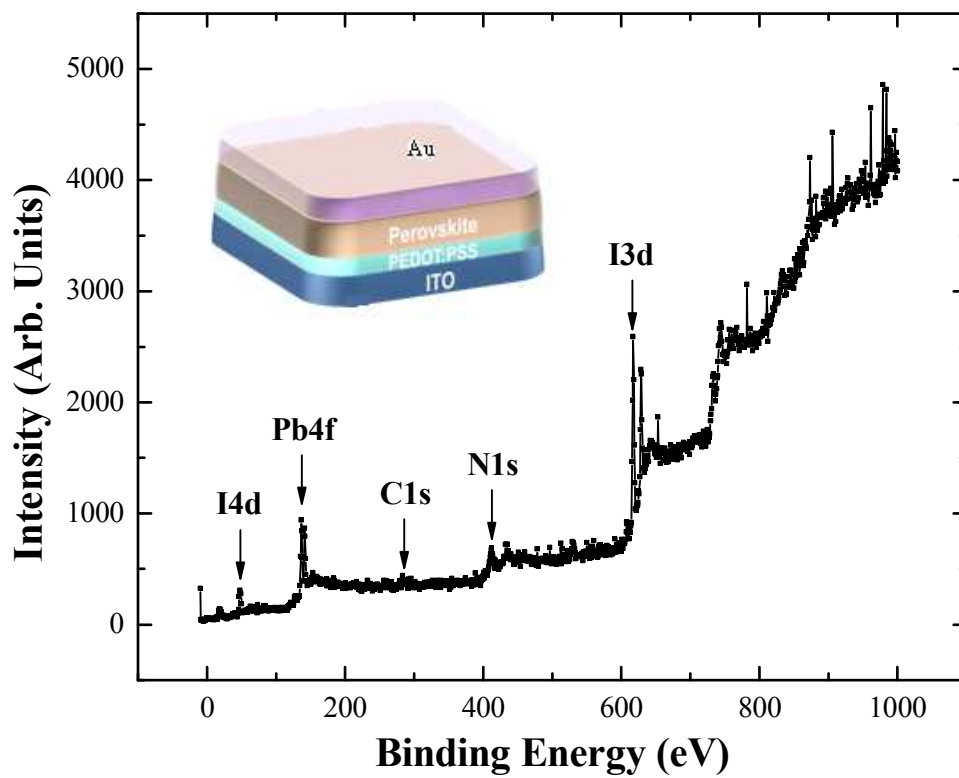


Fig. 1. X-ray photoelectron spectroscopy of the  $\text{CH}_3\text{NH}_3\text{PbI}_3$  film on the top of ITO/PEDOT:PSS substrate. Inset: the schematic diagram of the structure of ITO/PEDOT:PSS/ $\text{CH}_3\text{NH}_3\text{PbI}_3$ /Au.

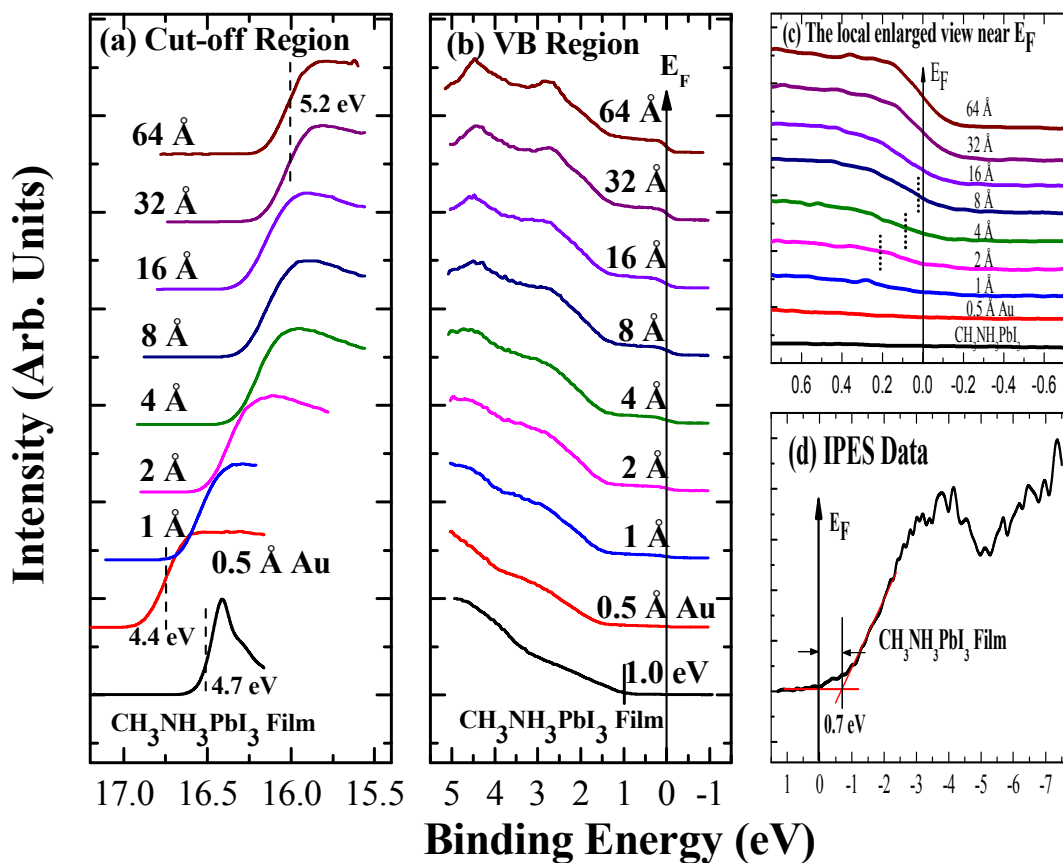


Fig. 2. Thickness dependent UPS spectra of Au on  $\text{CH}_3\text{NH}_3\text{PbI}_3$  coated on PEDOT:PSS/ITO substrate showing (a) the cut-off region, (b) the VB edge region, (c) the local enlarged view of the VB edge region near  $E_F$ . (d) presents IPES spectra of the density of states close to the bandgap of the  $\text{CH}_3\text{NH}_3\text{PbI}_3$ . Positions of the VB edge and the CB edge are marked with vertical bars, while positions of the cut-off energy and the Fermi edge are marked with dashed and dotted lines, respectively.

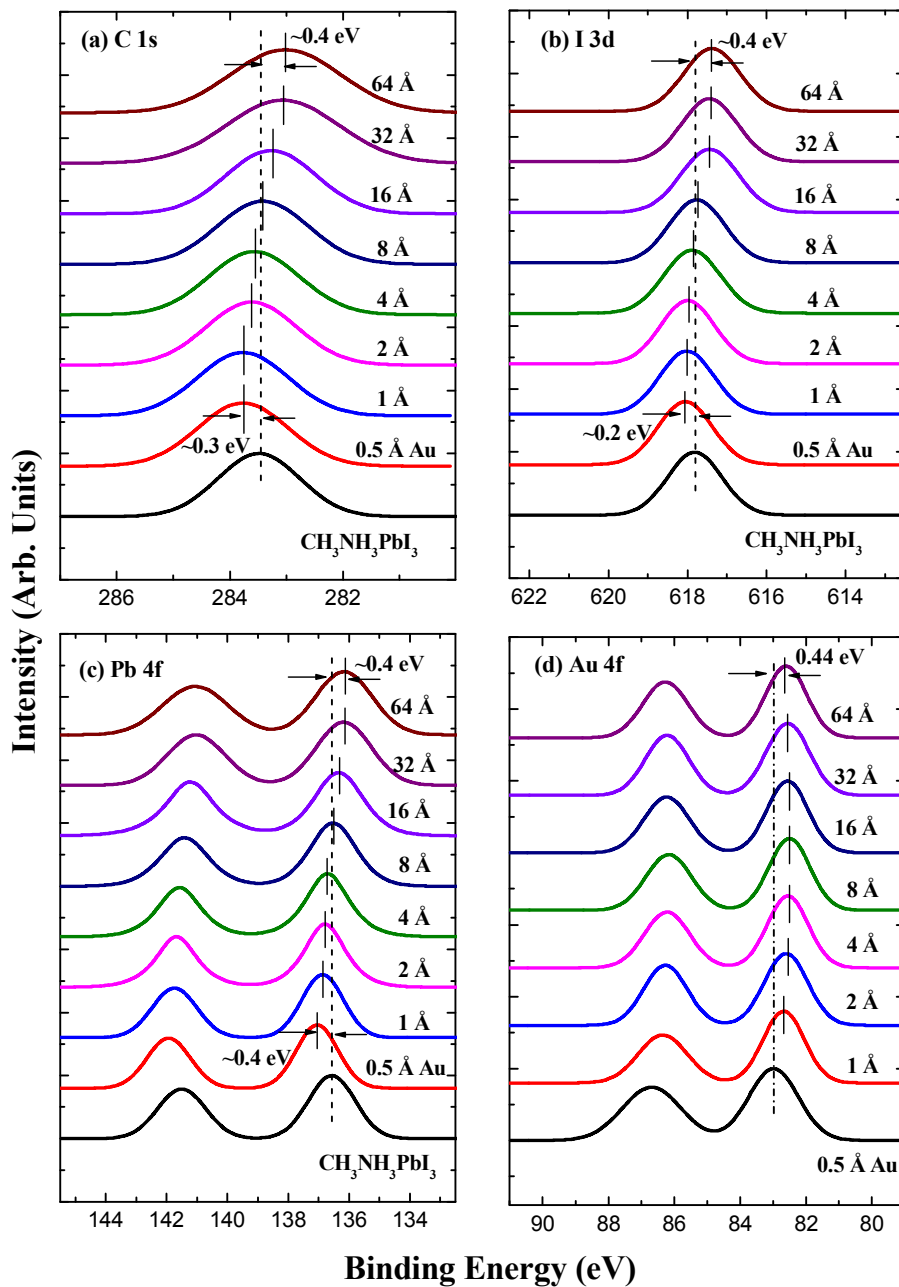


Fig. 3. The evolution of (a) C 1s, (b) I 3d and (c) Pb 4f XPS peaks in the  $\text{CH}_3\text{NH}_3\text{PbI}_3$  film, and that of (d) Au 4f XPS peaks in Au coverage, with the increasing Au coverage thickness.

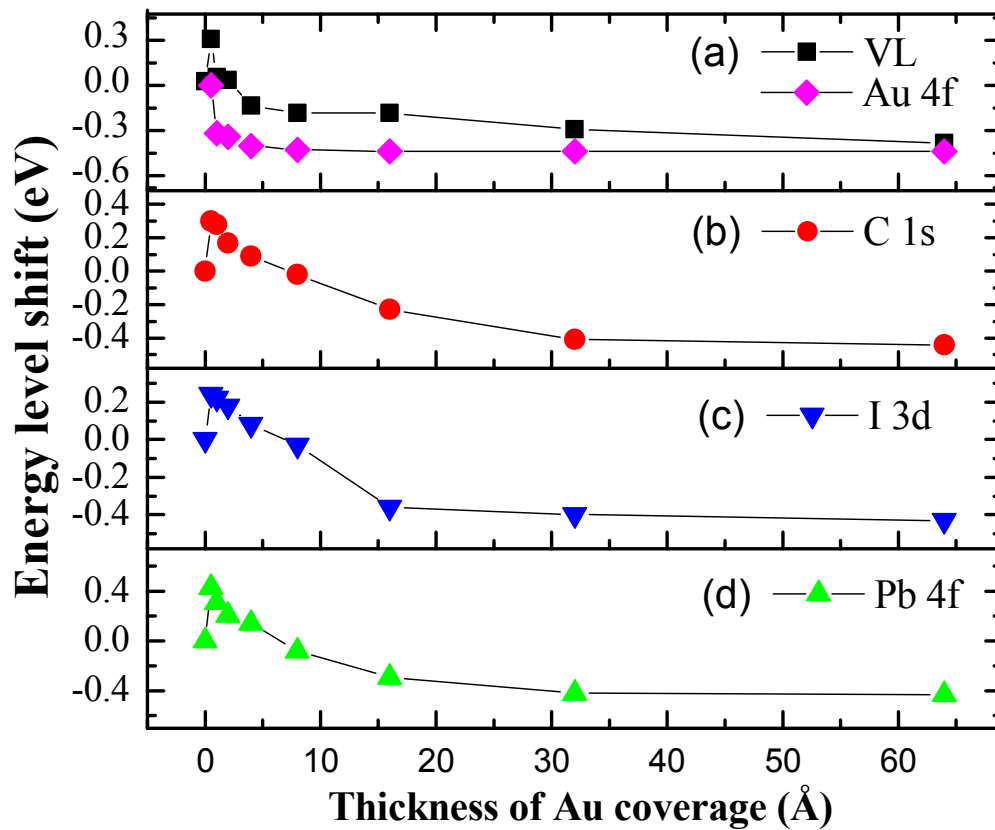


Fig. 4. The relative shifts of vacuum level and core levels at the  $\text{CH}_3\text{NH}_3\text{PbI}_3/\text{Au}$  interface deduced from UPS and XPS. The zero of the energy scale refers to the value of zero (or 0.5 Å for Au 4f) Au coverage.

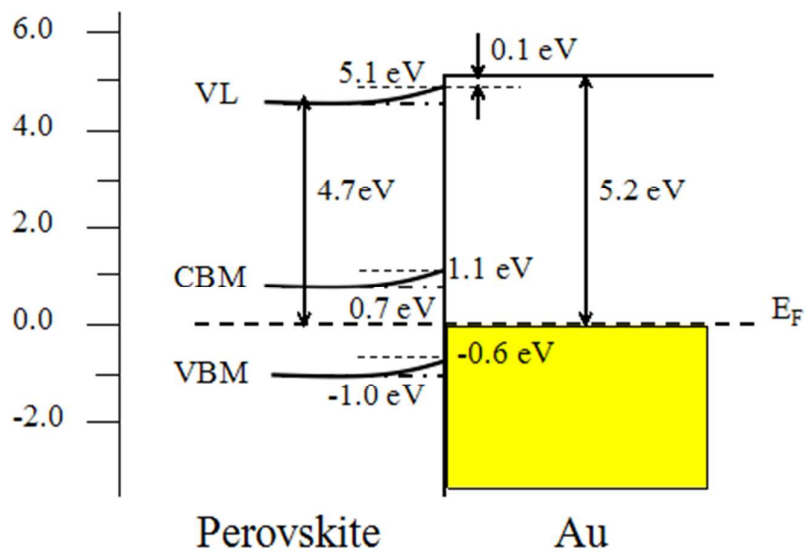


Fig. 5. The energy level diagram of  $\text{CH}_3\text{NH}_3\text{PbI}_3/\text{Au}$  interface. The dash dotted lines denote the energy levels of the pristine  $\text{CH}_3\text{NH}_3\text{PbI}_3$  film, while the solid lines on the side of  $\text{CH}_3\text{NH}_3\text{PbI}_3$  denote the evolution of the energy levels with the deposition of Au.

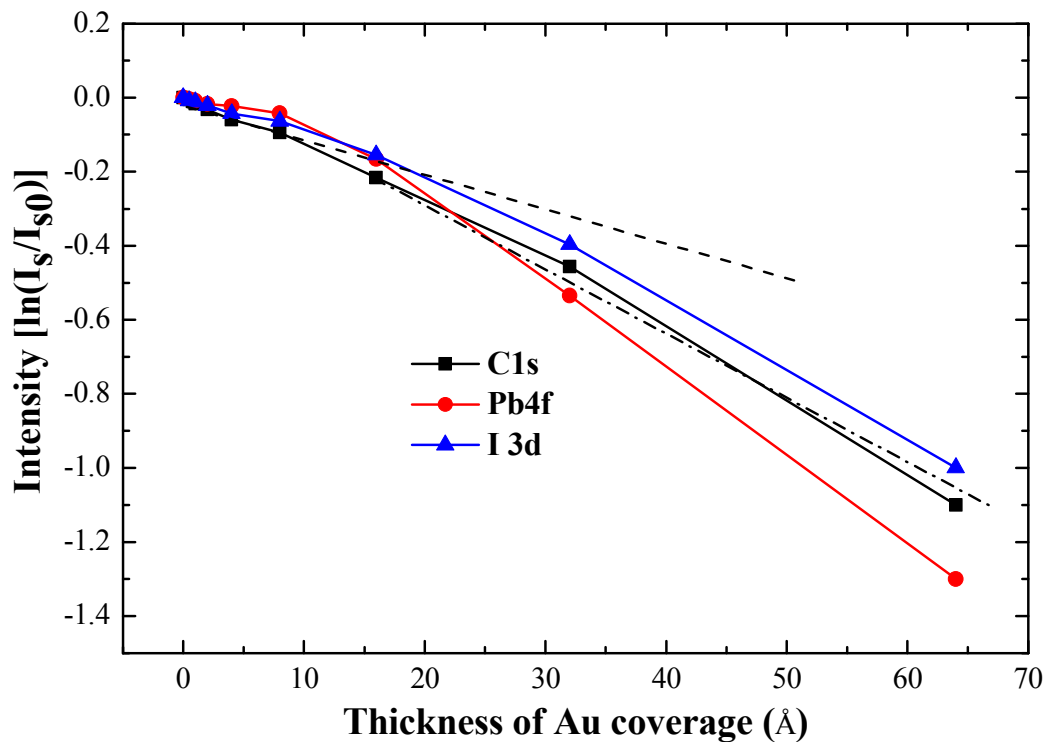


Fig. 6. The photoelectron intensity as a function of the thickness of Au coverage. The dash line and the dash dotted line mark the slopes for the C 1s before and after the Au deposition of 8 Å, respectively.



The electronic properties of interface formed between Au and organometal triiodide perovskite ( $\text{CH}_3\text{NH}_3\text{PbI}_3$ ) are investigated using photoemission spectroscopy.

